RSC Advances

ROYAL SOCIETY OF CHEMISTRY

www.rsc.org/advances

Journal Name

ARTICLE

First Principles Study on Electronic Property of Ni₃(2, 3, 6, 7, 10, 11-hexaaminotriphenylene)₂ monolayer under Biaxial Strain

De You Tie and Zheng Chen*

Applying first principles calculations, the electronic structure of $Ni_3(HITP)_2$ (HITP=2,3,6,7,10,11-hexaaminotriphenylene) monolayer have been investigated with both GGA and GGA+U methods. $Ni_3(HITP)_2$ monolayer is semi conductive with a narrow indirect band in an unstrained system. Under biaxial strain, our computation reveals that the monolayer become metallic after the band gap gradually decreases to zero with increased strain. The 2D sheet is verified to be typical π-conjugated characteristics with each Ni atom adopt the dsp^2 hybridization at zero strain. We demonstrates the variation of charge density of the monolayer to show the gradually weakening of the Ni-N bond as the strain increases. Our band structure and charge density analysis indicates the variation of band gap can be the result of charge redistribution between Ni and N atoms due to the biaxial strain applied.

1. Introduction

Monolayer nanosheet materials have changed the knowledge of material science since the mechanical exfoliation of graphene by Novoselov and Geim[1]. Many great efforts have been made to extend the research on their physical and chemical property derived from their two-dimensional (2D) nature. For example, graphene is one of the most prominent nanosheet materials with in-plane pi-conjugation[1], which has an extremely high electron mobility due to the linear dispersion relation in its band structure around the Dirac point[2]. However, the disadvantage of graphene is the application in semiconductor-based devices due to its zero bandgap [3-5]. Since the modification of graphene cannot perfectly solve this problem[6, 7], researchers start to focus on investigating other types of 2D nanosheet materials which exhibit similar electronic property without zero band gap, such as hexagonal BN sheet[8], transition metal dichalcogenides[9, 10], silicone[11], germanane[12] and metal organic frameworks[13-15].

With the advances in synthesis and experimental techniques, "top-down" and "bottom-up" are the most effective methods when those graphene analogues are considered[16-19]. Recently some of the "bottom-up" solution-based synthetic methods have showed that many sophisticated ligands bridging by certain metal ions exhibit non-zero bandgaps and considerable electrical conductivity in 2D plane[20]. Therefore, these 2D metal-organic networks described as semiconducting metal-organic graphene analogues (s-MOGs) seem to be promising for future electronics.

Inspired by the success of dithiolene-based s-MOGs, a new crystalline s-MOG with very high electrical conductivity called $Ni_3(HITP)_2$ (HITP=2,3,6,7,10,11-hexaaminotriphenylene) was synthesized and analysed as bulk powders and thin films[20]. Although the electronic property of 3D $Ni_3(HITP)_2$ bulks was found to be metallic recently, the monolayer framework turned out to be semi conductive[21], which made us wonder if there exists some methods to modify its band gap so that we could trigger some more interesting properties.

Instead of other various methods such as nanostructuring[22, 23], doping[24], chemical functionalization[25], the application of external electric field[26, 27], substrate absorption to break symmetry[28], the application of strain becomes our choice. A controlled introduction of biaxial strain provides a convenient and reversible way to investigate both the tuning of electronic structure and mechanical property at the same time, so that we are able to find out the connection between the band gap and the biaxial strain.

In this work, we investigated the basic geometric and electronic property of 2D $Ni_3(HITP)_2$ monolayer through its band structure. We also simulate the change of cell structure and electronic structure when the monolayer was applied increasing isotropic biaxial strain. In the end, we investigate the mechanism of how the biaxial strain effect the electronic structure.

2. Computational Details

Geometry optimizations were performed using the Vienna ab initio simulation package (VASP)[29, 30]. The exchange-correlation energy was described by the generalized gradient approximation (GGA) in the form of Perdew, Burke, and

State Key Laboratory of Solidification Processing, School of Material Science and Engineering, Northwestern Polytechnical University, 127 YouYi Western Road, Xi'an, Shaanxi 710072, China. E-mail: tiedeyou@hotmail.com

Ernzerhof (PBE)[31]. The electron-ion interactions were described by the projector-augmented wave (PAW) method with an energy cutoff of 400 eV (the convergence criteria is 0.01 eV), which is primarily a frozen-core all-electron calculation[32]. Spin-polarized GGA+U calculations were also performed with a U_{eff} value of 3 eV for the Ni ions since DFT often provides an unsatisfactory description for the strongly correlated transition-metal system with localized d subshells, which have been tested and used in previous theoretical studies[33]. We also checked the band structure with U_{eff} value of 4 eV and 5 eV to check the best value of U_{eff}. We applied the 2D periodic boundary condition with the unit cell forced into P6/mmm symmetry, and a vacuum space of 15 Å along the z direction was adopted to avoid the interactions between two layers in nearest-neighbouring unit cells. For the structure optimization, the atoms were relaxed in the direction of the Hellmann-Feynman force using the conjugate gradient method until a stringent convergence criterion (=0.03eV/ Å) was satisfied. Since our model was based on 2D $Ni_3(HITP)_2$ nanosheet, the Brillouin zone was represented by Monkhorst-Pack k-point mesh of 3×3×1 for geometry optimizations (the convergence criteria is 0.001 eV), and a large grid (9×9×1) was used for self-consistent calculations. The 3D bulk structure was also briefly calculated to be compared with the geometry structure of 2D nanosheet. The Monkhorst-Pack k-point mesh for geometry optimizations is set to be 2×2×6. The periodic 2D framework and 3D bulk were constructed under the consideration of previous work[20, 21].

3. Result and Discussion

3.1 2D $Ni_3(HITP)_2$ Nanosheet and 3D bulk structure

In the beginning we compare the geometric properties of strain-free monolayer nanosheet of $Ni_3(HITP)_2$ with its bulk structrure. The lattice parameter of $Ni_3(HITP)_2$ unit cell is optimized to be 21.96 Å, which is slightly bigger than 21.78 Å in bulk structure. We also identified the $Ni_3(HITP)_2$ monolayer is a porous material with a very large pore size of 19.695 Å (N-N)~20.633 Å (C-C) showed in Figure 1, and the Ni-N bond length (L_{Ni-N}), N-C bond length (L_{N-C}) are 1.838 Å and 1.357 Å, respectively. While in bulk structure, the pore size is 19.655 Å (N-N) ~20.452 Å (C-C) and the L_{Ni-N}, L_{N-C} are 1.820 Å and 1.358 Å. The comparison of the 2D and 3D structure of $Ni_3(HITP)_2$ indicates that the single layer of bulk is constrained since its 2D parameters are slightly larger than 3D parameters.

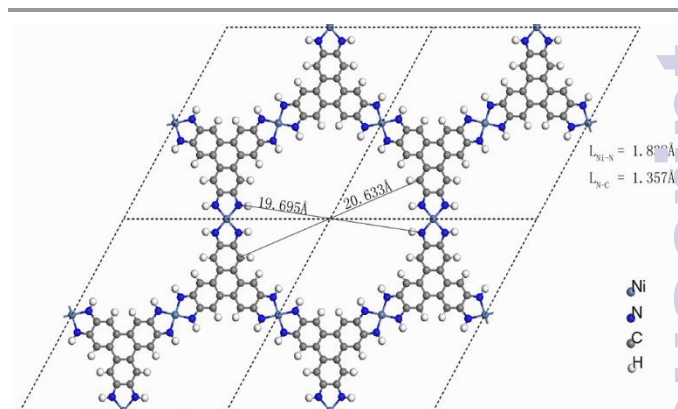**Figure 1.** Optimized structure of 2D $Ni_3(HITP)_2$ monolayer. The atoms of unit cell are forced into P6/mmm symmetry represented by the dashed rhombus. H atoms are used to terminate the edges.

Consisted with the work of Chen et al[21], Figure 2 depicts the monolayer $Ni_3(HITP)_2$ framework is predicted to be a semiconductor with an indirect band gap of 0.118 eV at the GGA level, slightly less than 0.128 eV at the GGA+U level (U_{eff} = 3 eV) due to the valance band maximum (VBM) decreases. As we increase the value of U_{eff} to 4 eV and 5 eV, the band gap increases to nearly 0.14 eV. Compared with ref.21, we believe U_{eff} = 3 eV is the most appropriate value in these calculations. This narrow band gap is much smaller than traditional semiconductors.
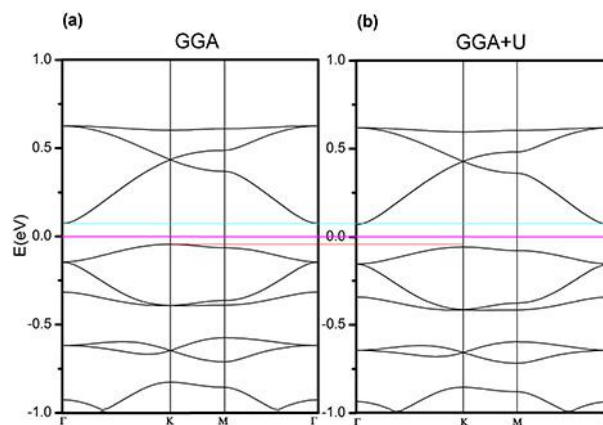

Figure 2. Computed band structure with GGA (a) and GGA+U (b) method. The Fermi level is marked by a thin Purple line while the blue and red line are used to show the change of conduction band minimum (CBM) and valance band maximum (VBM).

3.2 Biaxial Strain to $Ni_3(HITP)_2$ Monolayer

We choose to apply increasing biaxial tensile strain in plane which is defined by the relation $\varepsilon = (a - a_0)/a_0 \times 100$, where a and a_0 are the lattice parameters of strained and unstrained systems, respectively. In order to have a good understanding of the process, $\Delta\varepsilon$ is set to be 1%. The strain energy of each step is defined by the relation $E_s = E_\varepsilon - E_0$, where E_ε is the total energy of the strained unit cell and E_0 is the corresponding energy in equilibrium.

Figure 3 Shows the tuning of electronic structure has been achieved as we expected. Though there is no change of the nonmagnetic property, the electronic property is slowly

ARTICLE

effected by the magnitude of the applied strain. We find it interesting that the band gap decreases with the strain and become zero when ε is 7% in Figure 3(d). Figure 3 also demonstrates that the electronic property of 2D sheet changes from semi conductive into metallic due to its highest occupied valance band (HOVB) decreases and lowest unoccupied conduction band (LUCB) increases. The HOVB at K point increases from -0.0582 eV to 0 eV and the LUCB at Γ point decreases from 0.0696 eV to -0.0228 eV. The band gap vanishes due to the value of HOVB becomes higher than the value of LUCB at ε = 7%.

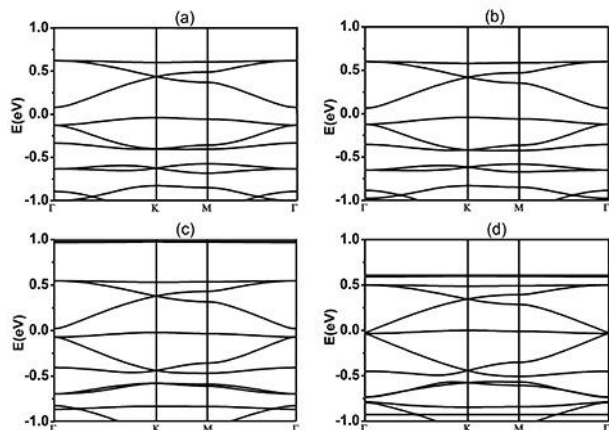**Figure 3.** Electronic band structure of the 2D $Ni_3(HITP)_2$ monolayer at ε = 1% (a), 3% (b), 5% (c) and 7% (d).

Recent research showed the delocalized d orbitals of Ni atoms provide contributions to both the HOVB and LUCB[21] indicating that Ni-N bond plays a key part in band gap variation as a function of the biaxial strain. Figure 4(a) and (b) present the computed DOS and PDOS of 2D $Ni_3(HITP)_2$ monolayer at ε = 0 and ε = 7%, respectively. Both of them show the band around Fermi level are mostly contributed from Ni-d, C-p and N-p orbitals. In Figure 4(a), density of states at HOVB and LUCB at ε = 0 are zero, while in Figure 4(b), density of states at the same positions increase to 0.44 and 1.18 states/eV. The unoccupied Fermi level at ε = 0 becomes occupied at ε = 7%, which indicates the change of band structure is mainly caused by the change of occupation at Fermi level.

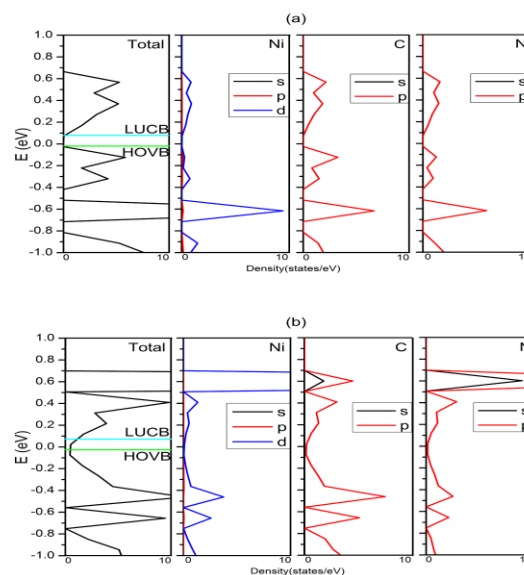**Figure 4.** The DOS and PDOS of 2D $Ni_3(HITP)_2$ monolayer at ε = 0 (a) and ε = 7% (b). Black, red and dark blue lines represent s, p and d orbitals of different atoms. LUCB and HOVB at ε = 0 are marked by light blue and green lines.

In order to understand the changes of PDOS at Fermi level, we focus on the bond length of Ni, N and C atoms as well as their charge density distribution. The 2D monolayer remains metallic when ε ≥ 7%. As the strain is increased, L_{Ni-N} and L_{N-C} changes as shown in Figure 5(b). It is obvious that L_{Ni-N} abrupt increases at ε = 9% while L_{N-C} decreases, and in Figure 5(a) the slope of E_s suddenly changes at ε = 8%, which indicates ε = 8% corresponds to the maximal biaxial strain before the fragmentation.
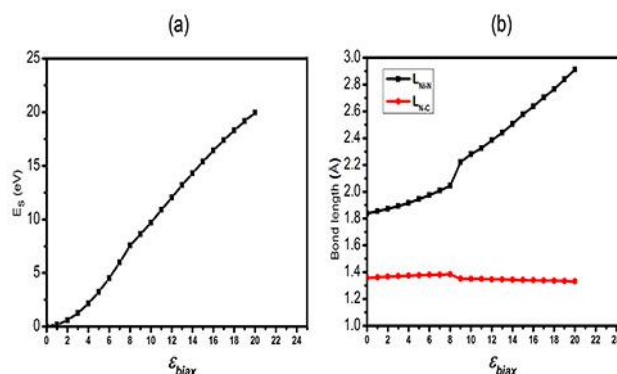

Figure 5. The strain energy (E_s) of each step (a) and the Ni-N (black), N-C (red) bond length (b) of the $Ni_3(HITP)_2$ monolayer as a function of the biaxial strain.

Figure 6(a) verifies that the 2D sheet exhibit typical π-conjugated characteristics with each Ni atom adopt the dsp^2 hybridization, which is in a good agreement with the earlier result[21]. Figure 6(b) (c) and (d) demonstrate the gradual redistribution of charge density as the strain increases. The increase of Ni-N bond length induces the charge density to redistribute more closely to Ni and N respectively, so that the weakening of Ni-N bond will be compensated. The extra charge Ni and N get will occupy more energy level which affect

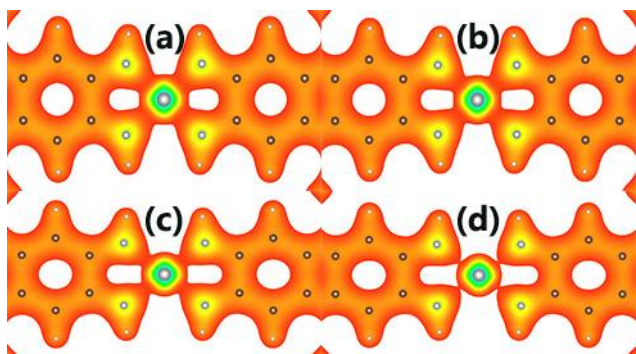the bottom of the HOVB and the top of the LUCB as the band gap decreases and Fermi level becomes occupied.

Figure 6. Charge density isosurface of the $Ni_3(HITP)_2$ monolayer at $\varepsilon = 0$ (a), 3% (b), 5% (c) and 7% (d) . The variation of colour green - yellow – red represents the decreasing level of charge density value. The isosurface value for charge density is 0.08 e/Bohr^3.

4. Conclusions

In this study, we investigated the electronic structure of 2D $Ni_3(HITP)_2$ monolayer under biaxial strain. We compared the electronic structure of the monolayer by using GGA and GGA+U methods at zero strain. The 2D sheet is semi conductive with a narrow indirect band of 0.128 eV when the system is in equilibrium. Under biaxial strain, our computation revealed the band gap of the monolayer gradually decreased with increased strain and became zero at $\varepsilon = 7\%$. Our DOS and PDOS analysis showed The unoccupied Fermi level at $\varepsilon = 0$ becomes occupied at $\varepsilon = 7\%$, which indicates the band structure changes is mainly caused by the occupation changes at Fermi level. The monolayer turned into fragment at $\varepsilon = 9\%$ as the Ni-N bond length abrupt increased and N-C bond length decreased. In the end we presented the variation of charge density of the monolayer. The 2D sheet is verified to be typical π-conjugated characteristics with each Ni atom adopt the dsp^2 hybridization at $\varepsilon = 0$. The charge density variation also showed the gradually weakening of the Ni-N bond as the strain increased. The band structure and charge density analysis indicated the variation of band gap could be ascribed to charge redistribution between Ni and N atoms due to the biaxial strain applied. Our work is just a small exploration of this new material. There are so much potential property to be discovered. This interesting property may inspire some other future application or experimental phenomenon. We hope our research will motivate more experimental and theoretical studies on this new developed material and its possible applications in nanoelectronics.

Acknowledgements

References

1　K. S. Novoselov, A. K. Geim, S. V. Morozov, D. Jiang, Y. Zhang, S. V. Dubonos, I. V. Grigorieva and A. A. Firsov, *Science*, 2004, **306**, 666.
2　A. K. Geim and K. S. Novoselov, *Nat. Mater*., 2007, **6**, 183.
3　K. S. Novoselov, A. K. Geim, S. V. Morozov, D. Jiang, M. I. Katsnelson, I. V. Grigorieva, S. V. Dubonos and A. A. Firsov, *Nature*, 2005, **438**, 197.
4　A. H. Castro Neto, F. Guinea, N. M. R. Peres, K. S. Novoselov and A. K. Geim, *Rev. Mod. Phys.,* 2009, **81**, 109.
5　P. Avouris, *Nano Lett.*, 2010, **10**, 4285.
6　P. Ruffieux, J. Cai, N. C. Plumb, L. Patthey, D. Prezzi, A. Ferretti, E. Molinari, X. Feng, K. Müllen, C. A. Pignedoli and R. Fasel, *ACS Nano*, 2012, **6**, 6930.
7　V. Georgakilas, M. Otyepka, A. B. Bourlinos, V. Chandra, N. Kim, K. C. Kemp, P. Hobza, R. Zboril and K. S. Kim, *Chem. Rev.*, 2012,**112**, 6156.
8　Y. Kubota, K. Watanabe, O. Tsuda and T. Taniguchi, *Science,* 2007, **317**, 932.
9　J. N. Coleman, M. Lotya, A. O'Neill, S. D. Bergin, P. J. King, U. Khan, K. Young, A. Gaucher, S. De, R. J. Smith, I. V. Shvets, S. K. Arora, G. Stanton, H.-Y. Kim, K. Lee, G. T. Kim, G. S. Duesberg, T. Hallam, J. J. Boland, J. J. Wang, J. F. Donegan, J. C. Grunlan, G. Moriarty, A. Shmeliov, R. J. Nicholls, J. M. Perkins, E. M. Grieveson, K. Theuwissen, D. W. McComb, P. D. Nellist and V. Nicolosi, *Science*, 2011, **331**, 568.
10　A. Splendiani, L. Sun, Y. Zhang, T. Li, J. Kim, C.-Y. Chim, G. Galli and F. Wang, *Nano Lett*., 2010, **10**, 1271
11　B. Lalmi, H. Oughaddou, H. Enriquez, A. Kara, S. Vizzini, B. Ealet and B. Aufray, *Appl. Phys. Lett.,* 2010, **97**, 223109.
12　E. Bianco, S. Butler, S. Jiang, O. D. Restrepo, W. Windl and J. E. Goldberger, *ACS Nano,* 2013, **7**, 4414.
13　T. Kambe, R. Sakamoto, K. Hoshiko, K. Takada, M. Miyachi, J.-H. Ryu, S. Sasaki, J. Kim, K. Nakazato, M. Takata and H. Nishihara, *J. Am. Chem. Soc*., 2013, **135**, 2462.
14　N. Abdurakhmanova, T.-C. Tseng, A. Langner, C. S. Kley, V. Sessi, S. Stepanow and K. Kern, *Phys. Rev. Lett*., 2013, **110**, 027202.
15　M. Abel, S. Clair, O. Ourdjini, M. Mossoyan and L. Porte, *J. Am. Chem. Soc.,* 2010, **133**, 1203.
16　K. F. Mak, C. Lee, J. Hone, J. Shan and T. F. Heinz, *Phys. Rev. Lett.,* 2010, **105**, 136805.
17　M. Chhowalla, H. S. Shin, G. Eda, L.-J. Li, K. P. Loh and H. Zhang, *Nat. Chem.,* 2013, **5**, 263.
18　R. Gutzler and D. F. Perepichka, *J. Am. Chem. Soc.,* 2013, **135**, 16585.
19　J. W. Colson and W. R. Dichtel, *Nat. Chem.,* 2013, **5**, 453.
20　D. Sheberla, L. Sun, M. A. Blood-Forsythe, S. Er, C. R. Wade, C. K. Brozek, A. n. Aspuru-Guzik and M. Dincă, *J. Am. Chem. Soc.,* 2014, **136**, 8859.
21　S. Chen, J. Dai and X. C. Zeng, *Phys. Chem. Chem. Phys.*, 2015, DOI: 10.1039/C4CP05328A.
22　X. Li, X. Wang, L. Zhang, S. Lee and H. Dai, *Science*, 2008, **319**, 1229.
23　M. Y. Han, B. Özylmaz, Y. Zhang and P. Kim, *Phys. Rev. Lett.,* 2007, **98**, 206805.
24　Y. Gong, Z. Liu, A. R. Lupini, G. Shi, J. Lin, S. Najmaei, Z. Lin, A. L. Elías, A. Berkdemir, G. You, H. Terrones, M. Terrones,; R. Vajtai, S. T. Pantelides, S. J. Pennycook, J. Lou, W. Zhou and P. M. Ajayan, *Nano Lett*., 2014, **14**, 442.

25 R. Balog, B. Jørgensen, L. Nilsson, M. Andersen, E. Rienks, M. Bianchi, M. Fanetti, E. Lægsgaard, A. Baraldi, S. Lizzit, Z. Sljivancanin, F. Besenbacher, B. Hammer, T. G. Pedersen, P. Hofmann and L. Hornekær, *Nat. Mater.,* 2010, **9**, 315.
26 Y. Li and Z. Chen, *J. Phys. Chem. C.,* 2014, **118**, 1148.
27 A. Klien, S. Tiefenbacher, V. Eyert, C. Pettenkofer and W. Jaegermann, *Phys. Rev. B*, 2001, **64**, 205416.
28 S. Y. Zhou, G.-H. Gweon, A. V. Fedorov, P. N. First, W. A. DeHeer, D.-H. Lee, F. Guinea, A. H. Castro Neto and A. Lanzara, *Nat. Mater.,* 2007, **6**, 770.
29 G. Kresse and J. Hafner, *Phys. Rev. B*, 1993, **47**, 558.
30 G. Kresse and D. Joubert, *Phys. Rev. B,* 1999, **59**, 1758.
31 J. P. Perdew, K. Burke and M. Ernzerhof, *Phys. Rev. Lett.,* 1996, **77**, 3865.
32 G. Kresse and J. Furthmüller, *Phys. Rev. B,* 1996, **54**, 11169.
33 J. Zhou and Q. Sun, *J. Am. Chem. Soc.,* 2011, **133**, 15113.

RSC Advances Accepted Manuscript

ARTICLE

Journal Name

Graphic Abstract
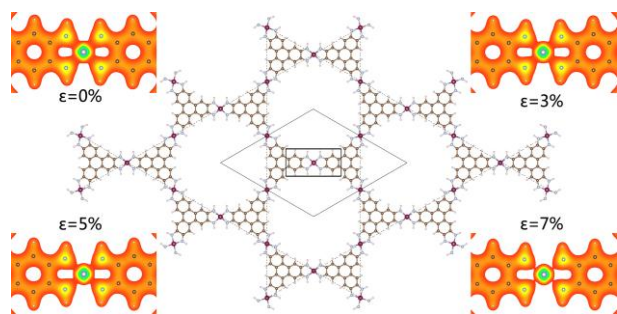
Electronic property of 2D π-conjugated $Ni_3(HITP)_2$ monolayer changes from semi conductive into metallic due to charge redistribution under biaxial strain.